The Sagittarius dwarf galaxy has a disk with a $\wedge$-like metallicity profile

Zixi Guo[1,3†], Xiang-Xiang Xue[1,2*†], Chao Liu[1,2,3*], Jiang Chang[4], Zehao Zhong[3], Bingqing Zhang[1], Shi Shao[1], Ruizhi Zhang[1], Zhuohan Li[1,3], Jianhui Lian[5], Haining Li[1], Ruizheng Jiang[1,3], Gang Zhao[1,3*]

[1]National Astronomical Observatories, Chinese Academy of Sciences, Beijing, 100101, China.
[2]Institute for Frontiers in Astronomy and Astrophysics, Beijing Normal University, Beijing, 102206, China.
[3]School of Astronomy and Space Science, University of Chinese Academy of Sciences, Beijing, 100049, China.
[4]Purple Mountain Observatory, Chinese Academy of Sciences, Nanjing, 210023, China.
[5]South-Western Institute for Astronomy Research, Yunnan University, Kunming, 650091, China.

*Corresponding author(s). E-mail(s): xuexx@nao.cas.cn; liuchao@nao.cas.cn; gzhao@nao.cas.cn;
†These authors contributed equally to this work.

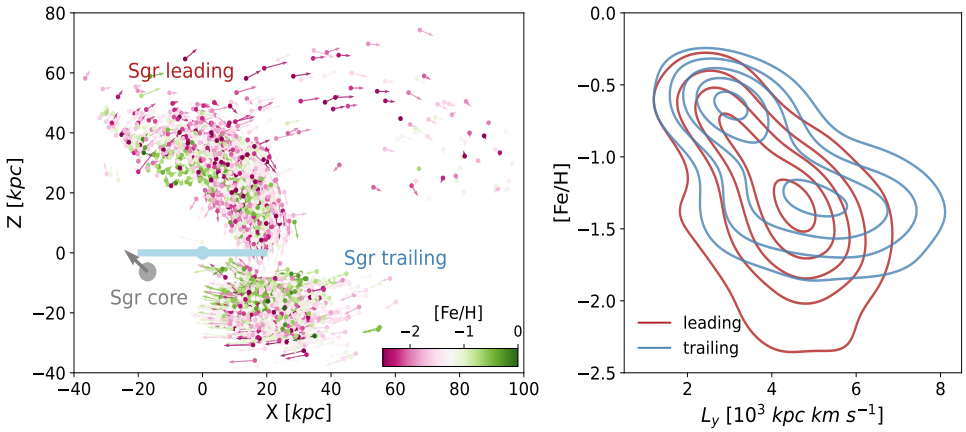

Fig. 1 Distribution of the Sgr stream members. Left panels: The spatial distribution of Sgr leading arm and trailing arm in the Galactocentric coordinate system. Milky Way disc plane is shown by blue line, and its center by a blue dot. The grey dot represents the position of Sgr core and the grey arrow indicates the direction of its movement. Arrows represent the Sgr stars' moving directions and velocity amplitudes, and every star is color-coded according to its metallicity. **Right panel:** $[Fe/H] - L_y$ correlation. The red contour and the blue contour represent the distribution of the leading arm and the trailing arm, respectively. We can see L_y and $[Fe/H]$ have a correlation in both the leading arm and the trailing arm.

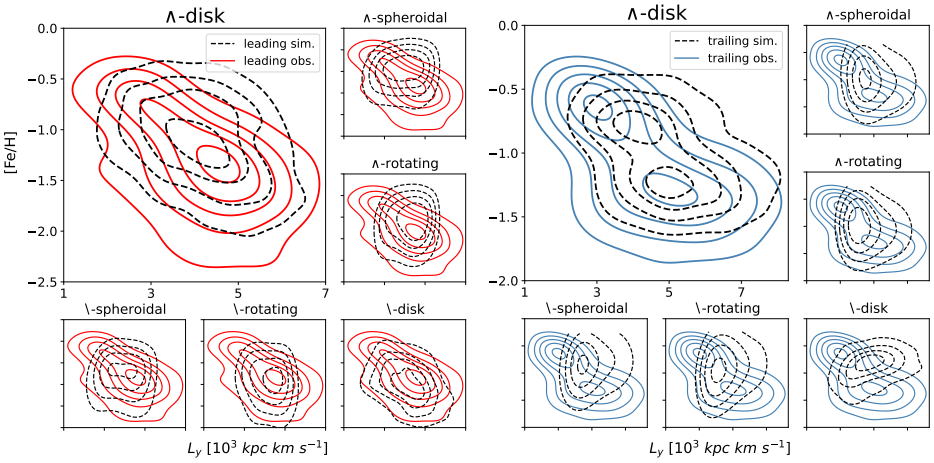

Fig. 2 Our simulations revealed the progenitor of Sgr stream. Left panel: The red and black contours represent the observation data and the mock data of the leading arm. **Right panel:** The blue and black contours represent the observation data and the mock data of the trailing arm. We discuss the distinctions of different models. Only the ∧-disk model can generate the $[Fe/H] - L_y$ correlation similar to the observation.

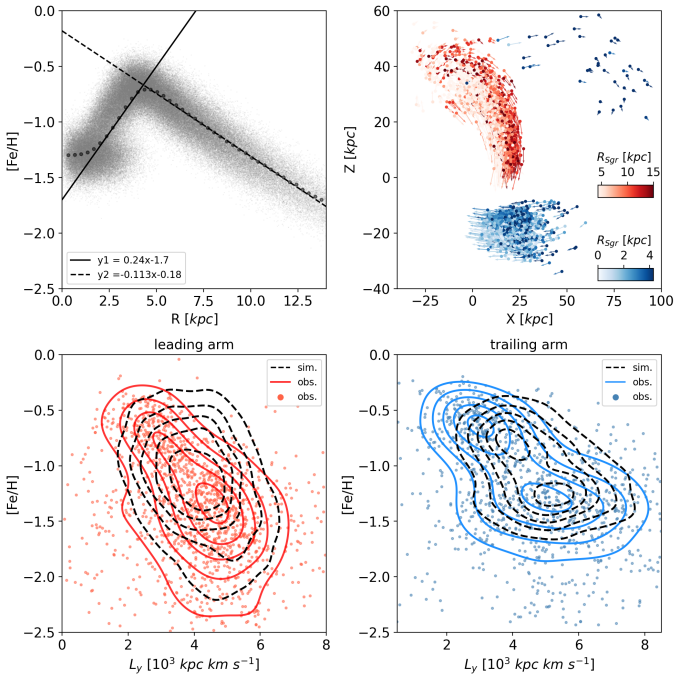

Fig. 3 Comparison between observation and the fiducial model. Top left: Initial metallicity profile of Sgr disk in the simulation. The gray dots represent the distance of the stellar particles from the center of Sgr and their metallicity in the initial condition. The dotted line represents the average metallicity at each radius. The dashed line and the solid line represent the metallicity gradients of the progenitor, with their slopes being -0.113 dex/kpc and 0.24 dex/kpc. **Top right:** Red and blue points respectively represent the leading and trailing arms in the mock data, with arrows indicating particle motion directions. The R_{sgr} encodes the distance between particles and the progenitor's center in initial conditions, where a deeper blue or red coloration corresponds to a larger radial distance. **Bottom left:** The Red contour and red dots represent the observation data and the black contour indicates the $[Fe/H] - L_y$ correlation of the leading arm in the simulation. **Bottom right:** The Blue contour and blue dots represent the observation data, and the black contour indicates the $[Fe/H] - L_y$ correlation of the trailing arm in the simulation. We can see that the mock data and the observation data have similar slopes for both the leading arm and the trailing arm.

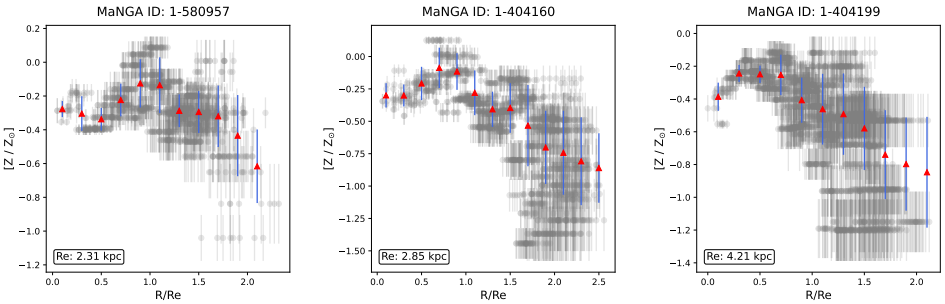

Fig. 4 A few dwarf galaxies with clearly Λ-like radial metallicity distribution from MaNGA survey. The radial bin values represent the light-weighted average of $Z_{\star,L}$ in concentric elliptical annuli spaced at 0.2 R_e intervals centered on the galaxy's optical center. The error bars of radial bins are contributed by the error propagation of each spaxel and the standard deviation within the elliptical annuli.

1 Method

1.1 Data

In our Sgr samples, we eliminate some stars with relatively large observational errors and retain the stars satisfying the following conditions: $d_{err}/d < 0.2$, $v_{los\_err} < 15\ km/s$, $[Fe/H]_{err} < 0.25\ dex$. Among the selected samples, 1443 stars are classified as leading arm and 1187 stars as trailing arm.

Considering that observational data contains errors, we are unable to make a direct comparison between the observational data and the simulation results. The errors associated with the $[Fe/H] - L_y$ correlations primarily stem from the uncertainties in line-of-sight velocity(v_{los}), distance modulus, and metallicity. In our simulations, the distance modulus error of stellar particles is approximately 10%, which is comparable to that in the observational data[1]. The errors in metallicity and v_{los} are established at 0.12 dex and 5 km/s, respectively. Subsequently, we will select the stellar particles that closely match the position and velocity of the observation data to serve as mock data from the snapshot. Figure 5 shows the mock data of the fiducial model, and we can discover a vertical metallicity gradient analogous to the observation.

In Figure 3, we can observe that the mock data of the leading arm and the trailing arm exhibit slight deviations from the observation in the $L_y - [Fe/H]$ space. Using a static gravitational potential and supposing that Sgr does not ingress into the Milky Way from a remote position(e.g. virial radius) would cause Sgr not to undergo adequate dynamical friction in the simulation. Consequently, the distribution range of L_y in the mock data would be smaller than that in the observed data. However, in Figure 3, we can see that the overall tendency of the mock data is consistent with the observational data, which suffices to demonstrate that the progenitor galaxy of Sgr is a disk galaxy.

1.2 Simulation details

In this simulation, we use a static Milky Way potential that includes both dark matter and stellar components. The dark matter halo of the Milky Way is described as a spherically symmetric Navarro-Frenk-White (NFW) potential[2] with virial mass $M_{vir} = 1 \times 10^{12} M_\odot$ and scale length $r_s = 19\ kpc$. The stellar component comprises a Miyamoto-Nagai disk ($6.8 \times 10^{10} M_\odot$) exhibiting scale length $R_s = 3\ kpc$ and scale height $R_h = 0.28\ kpc$[3], coupled with an exponentially truncated power-law bulge characterized by a power-law exponent of -1.8 and a cut-off radius of 1.9 kpc[4].

The current position of Sgr and its line-of-sight velocity in the International Celestial Reference System(ICRS) frame are $(ra, dec, D) = (283.76°,\ -30.48°,\ 26.0\ kpc)$ and $r_v = 142\ km\ s^{-1}$, and its mean proper motion is $\mu_\alpha = -2.7\ mas\ yr^{-1}, \mu_\delta = -1.35\ mas\ yr^{-1}$[5, 6]. Adopting Solar parameters from[7] ($X = (8,\ 0,\ 0)\ kpc$, $V = (-11.7,\ 241.63,\ 7.67)\ km\ s^{-1}$), we derive the Galactocentric position and velocity of the Sgr core as $X_{Sgr} = (-17.1,\ 2.46,\ -6.33)\ kpc$, $V_{Sgr} = (-234.53,\ -22.92,\ 205.04)\ km\ s^{-1}$. In our simulation, Sgr will pass through the pericenter four times. We apply the Gauss-Newton iteration method to find the initial coordinate of Sgr ~ 3.4 years ago[8, 9].

The disk progenitor is modeled as a composite system containing an exponential stellar disk and a Hernquist-profile dark matter halo[10], generated using the GalIC code[11]. Given the $[Fe/H]-L_y$ correlation's primary dependence on progenitor rotation, the bulge component is intentionally omitted. The simulations are conducted using the Gadget-2 code with 4×10^5 particles[12]. Detailed parameters of the fiducial model can be found in the Table 1.

Table 1 Parameters of Fiducial Model (3.4 Gyrs ago)

Component	Parameter	value
DM halo (Hernquist)	mass,$M_{200}(10^{10}M_\odot)$	2
	concentration	10
Disk (Exponential)	mass$(10^8M_\odot)$	8
	scale length(kpc)	2.5
	scale height(kpc)	0.75

In order to investigate how the various characteristics of the progenitor galaxy are reflected in the stellar stream, we also simulate with the other models–spheroidal galaxy and rotating elliptical galaxy, which have the same dark matter halo as the fiducial model. The detailed parameters of the models' stellar components are presented in Table 2. a/c is the stretch factor, and a = b and c are the axes of some isodensity ellipsoid. A prolate galaxy has $a/c<1$, while an oblate galaxy has $a/c>1$. The parameter k,

$$\langle v_\phi\rangle^2 = k^2[\langle v_\phi^2\rangle - \sigma_R^2]$$

, is used to delineate σ_ϕ^2. If we assume k to be 0, then this galaxy is a non-rotating system.

Table 2 Parameters of Spheroidal Model and Rotating Elliptical Model

Galaxy	Stellar Mass	Scale length(a)	Stretch(a/c)	k
Spheroidal	$8\times10^8M_\odot$	1.53 kpc	1	0
Rotating elliptical	$8\times10^8M_\odot$	2.29 kpc	2	1

1.3 Disk model

In the disk model, through extensive parameter space exploration, we identify multiple factors influencing the Sgr stream, including MW potential, LMC, and the Sgr progenitor. Given the prohibitive computational cost required for exhaustive parameter space exploration, we focus on the following key parameters exhibiting dominant control over $[Fe/H]-L_y$ correlation:(1) spin angular momentum vector, (2) mass and scale length of the disk, (3) initial metallicity profile.

1.3.1 Spin angular momentum vector(L_{spin})

In the Galactocentric rest frame, we generate an initial disk whose $L_{spin,0}$ is in the positive direction of the z-axis, and then we use the following matrices to rotate it.

$$\mathbf{R_x(i)} = \begin{bmatrix} 1 & 0 & 0 \\ 0 & cos(i) & -sin(i) \\ 0 & sin(i) & cos(i) \end{bmatrix} \tag{1}$$

$$\mathbf{R_z(i)} = \begin{bmatrix} cos(i) & -sin(i) & 0 \\ sin(i) & cos(i) & 0 \\ 0 & 0 & 1 \end{bmatrix} \tag{2}$$

For example, if we rotate $L_{spin,0}$ around the x-axis by an angle of $i \simeq -80°$ to get L_{spin}, the orbital angular momentum(L_{orb}) of Sgr and L_{spin} will be in the same direction. Our study holds that the included angle between L_{orb} and the positive direction of the z-axis is $\alpha = 80°$. We define the angle subtended by L_{spin} and L_{orb} as $\theta \equiv arccos[L_{orb} \cdot L_{spin}]$ with a range of 0 to 180 degrees and a free angle as ϕ with a range of 0 to 360 degrees[13, 14]. L_{spin} can be depicted using the following formula:

$$L_{spin} = R_x(-\alpha)R_z(\phi)R_x(\theta)L_{spin,0} \tag{3}$$

For θ and ϕ, we conduct 162 simulations with 20-degree increments and determine the optimal parameters of our fiducial model to be $\theta = 150°$ and $\phi = 40°$. Figure 6 and Figure 7 show the correlation between $[Fe/H]$ and L_y with different θ, and we set ϕ at 0° in these two figures. We establish that θ exerts significant control over the emergence of the $[Fe/H] - L_y$ correlation. This causal relationship originates from θ which critically governs the tidal interaction strength during galactic mergers. At $\theta \to 0°$, enhanced tidal stripping produces extended, filamentary streams through violent disk shocking; Conversely, $\theta \to 180°$ configurations yield thicker streams due to moderated interaction strength[15]. Our simulations show that a thick and metallicity-stratified stellar stream aligns more with the current observational data and θ can be restricted within the range of 130° to 170°. Although θ can be constrained relatively well, we cannot determine the range of ϕ through the $[Fe/H] - L_y$ correlation, as their relationship in our simulations shows no clear systematic pattern.

1.3.2 Initial metallicity profile

In this section, we test the influence of initial metallicity profile on the $[Fe/H] - L_y$ correlation. Before carrying out the simulation, we take the parameters of the fiducial model as the initial condition and set the metallicity for each particle of the disk within a coordinate system where the z-axis is in the same direction as L_{spin} and the center is at the center of Sgr progenitor. The metallicity of individual particles conforms to

the subsequent distribution.

$$[Fe/H] \sim \begin{cases} N_1(\mu_1, \sigma_1) & comp.1,\ p_1 = max\{1 - l_z/a, 0\} \\ N_2(\mu_2, \sigma_2) & comp.2,\ p_2 = min\{l_z/a, 1\} \end{cases} \tag{4}$$

where,

$$\mu_2 = \begin{cases} k_1(l_z - b) - 0.6 & (l_z < b) \\ -k_2(l_z - b) - 0.6 & (l_z \geq b) \end{cases} \tag{5}$$

Regarding other parameters, we take $\mu_1 = -1.3\ dex, \sigma_1 = 0.12\ dex, \sigma_2 = 0.1\ dex, a = 1.8\ [10^2\ km^2\ s^{-1}]$, and $b = 2\ [10^2\ km^2\ s^{-1}]$. k_1 and k_2 are free parameters. p_1 and p_2 represent the probabilities that a stellar particle with an angular momentum of l_z in the progenitor coordinate system follows the Gaussian distribution N_1 with a probability of p_1 and the Gaussian distribution N_2 with a probability of p_2. From the simulation results, we discover that k_1 predominantly influences the trailing arm, whereas k_2 mainly affects the leading arm. Figure 8 presents the initial metallicity profiles and the $[Fe/H] - L_y$ correlations in the simulations under different k_1. It can be observed that the trailing arm has two high-density regions. The metal-poor high-density region is mainly contributed by *comp.*1 of equation 4. Another high-density region comes from the stellar particles with high metallicity within a radius of 5 *kpc*. Therefore, a small k_1 would result in an indistinct $[Fe/H] - L_y$ correlation. And in Figure 9, we only vary the value of k_2. We find that if k_2 is too small, the leading arm in the simulation will lack metal-poor stellar particles. Based on the observation and simulation data, we constrain that k_1 must be greater than 0.15, and k_2 must be bigger than 0.15 and less than 0.25.

1.3.3 Mass and scale length of Sgr disk

In order to impose better constraints on the disk of Sgr, we examine the influence of scale length and mass on the $[Fe/H] - L_y$ correlation. When we test the impact of the scale length, the disk models are initialized with scale lengths of 1.5 *kpc*, 2 *kpc*, 2.5 *kpc*, 3 *kpc*, and 3.5 *kpc*. In diverse models, a and b determine whether the $[Fe/H] - L_y$ correlation emerges. Therefore, a rational parameter a and b will be selected for each model, while the other parameters are identical to those in the fiducial model, and we set $k_1 = 0.36$ and $k_2 = 0.22$. Figure 10 indicates that the trailing arm will lack metal-poor components caused by the smaller disc. Under the same mass, a smaller disk would lead to a deeper gravitational potential in the central region, making it more difficult for the central metal-poor particles to escape. Consequently, there will also be a deficiency of metal-poor stellar particles in its trailing arm.

In the subsequent test, we exclusively adjust the stellar mass, whereas all other parameters are held constant. From Figure 11, it can be inferred that a greater stellar mass would also give rise to a deficiency of metal-poor components in the trailing arm. According to our simulation results, either a significantly short scale length or an excessively large stellar mass is insufficient to produce a $[Fe/H] - L_y$ correlation. Consequently, we contend that in our simulation, the scale length of the Sgr disk should exceed $2kpc$, and the proportion of stellar mass to total mass should remain below 0.08.

1.4 Comparison of disk model, spheroidal model and rotating elliptical model

In this section, we compare the stellar streams generated by the fiducial model and the other two galaxies. For the spheroidal model and rotating elliptical model, it is not a preferable option to mark the metallicity of each particle according to l_z like the equation 4. We employ r to substitute for l_z in the spheroidal model and, $\widetilde{r} = \sqrt{R^2 + (a/c)^2 z^2}$ in the rotating elliptical model. These three models all have the $\wedge$-like metallicity profile.

To investigate the causes of the $[Fe/H] - L_y$ correlation, we analyze all the particles of three models within the observation area and do not add errors to the simulated data. Figure 12 presents the distributions of leading arms and trailing arms in the $[Fe/H] - L_y$ space produced by various models, and the color of each point represents the average stripped time of the particles in this bin.

From the disk model in Figure 12, we can discover that the $[Fe/H] - L_y$ correlation is composed of stellar particles that were stripped from different periods, and stellar particles characterized by distinct stripped times have different angular momenta and metallicity. However, in the spheroidal model, this distinction of angular momentum and metallicity is not obvious, attributed to low rotating velocity and large velocity dispersion of progenitor. From the spheroidal model to the rotating elliptical model and then to the disk model, the $[Fe/H] - L_y$ correlation becomes progressively more pronounced, suggesting that the Sgr progenitor might have been a galaxy mainly supported by rotation.

1.5 Searching dwarf galaxies with $\wedge$-like metallicity profile from MaNGA survey

The Mapping Nearby Galaxies at Apache Point Observatory (MaNGA) is one of the state-of-art widely used galaxy surveys[16], which provides spatially resolved spectra that includes both the kinematics and chemical information of galaxies. The `pipe3D` pipeline perform a continuum segmentation binning method to produce higher-S/N average spectra[17], which have been used to analyze stellar population for more than 10,000 galaxies in the MaNGA survey[18]. We made use of the spatially resolved stellar population information from `pipe3D` value added catalogues to search dwarf galaxies with $\wedge$-like metallicity distribution. The dwarf galaxies here refer to galaxies with logarithmic stellar mass $log(M/M_{\odot})$ less than 9.5. Based on this, we utilised dwarf galaxies from MaNGA survey with stellar mass less than or equal to $9.5 - \log(2)$ within the petrosian r-band effective radius $R_{\rm e}$, simply assuming that the mass-to-light ratios of these galaxies are constant from the inside to the outside. In addition, to ensure the observed field of view (FoV) can cover most area of galaxies, we only utilised dwarf galaxies with the diagonal radius of the integral field unit (IFU) cube larger than or equal to $2R_{\rm e}$ (FoV $\geq$ 2R$_{\rm e}$). Moreover, we only used the observation of 9l and 127 fibers to ensure sufficient data points for the sample. After these steps, we finally got a sample of 217 dwarf galaxies.

Among this sample, we used the spatial resolved light-weighted $Z_{\star,L}$ map of each dwarf galaxy to calculate the radial metallicity distribution. We only select galaxies with $\wedge$-like distribution peaks between $0.5R_e$ and $1.5R_e$. In addition, we tend to exclude edge-on dwarf galaxies, because they have less IFU spaxels at the same stellar mass, and their $\wedge$-like metallicity distributions are more difficult to confirm. We excluded some plausible samples, and finally selected three dwarf galaxies with clearly $\wedge$-like metallicity distribution by visual inspection and as shown in Figure 4.

Data availability

Most of the Sagittarius members used in this paper are publicly available from https://cdsarc.cds.unistra.fr/viz-bin/cat/J/ApJ/886/154. The catalogue used in this paper is hosted at https://zenodo.org/uploads/15493288. The data of pipe3D value-added catalogues of MaNGA survey used for this study are publicly available at https://data.sdss.org/datamodel/files/MANGA_PIPE3D/MANGADRP_VER/PIPE3D_VER/SDSS17Pipe3D.html

Code availability

The GADGET code for N-body simulation is available at https://wwwmpa.mpa-garching.mpg.de/galform/gadget/. The GALIC code for the construction of N-body galaxy models in collisionless equilibrium is available at https://wwwmpa.mpa-garching.mpg.de/~volker/galic/.

Acknowledgements

This study is supported by the National Key R&D Program of China Nos. 2024YFA1611902, 2024YFA1611903, 2023YFE0107800, the National Natural Science Foundation of China under grant Nos. 12588202, 12373020, the Strategic Priority Research Program of Chinese Academy of Sciences grant Nos. XDB1160102, and CAS Project for Young Scientists in Basic Research grant No. YSBR-062 and No. YSBR-092. We have m.de use of data from the European Space Agency (ESA) mission *Gaia* (https://www.cosmos.esa.int/gaia), processed by the *Gaia* Data Processing and Analysis Consortium (DPAC, https://www.cosmos.esa.int/web/gaia/dpac/consortium). Funding for the DPAC has been provided by national institutions, in particular the institutions participating in the *Gaia* Multilateral Agreement.

Guoshoujing Telescope (the Large Sky Area Multi-Object Fiber Spectroscopic Telescope LAMOST) is a National Major Scientific Project built by the Chinese Academy of Sciences. Funding for the project has been provided by the National Development and Reform Commission. LAMOST is operated and managed by the National Astronomical Observatories, Chinese Academy of Sciences.

Author contributions

Z.-X. G. contributed most of the modelling and provided simulation data. X.-X. X. proposed and initiated this study. C. L. developed the initial idea. G. Z. contributed

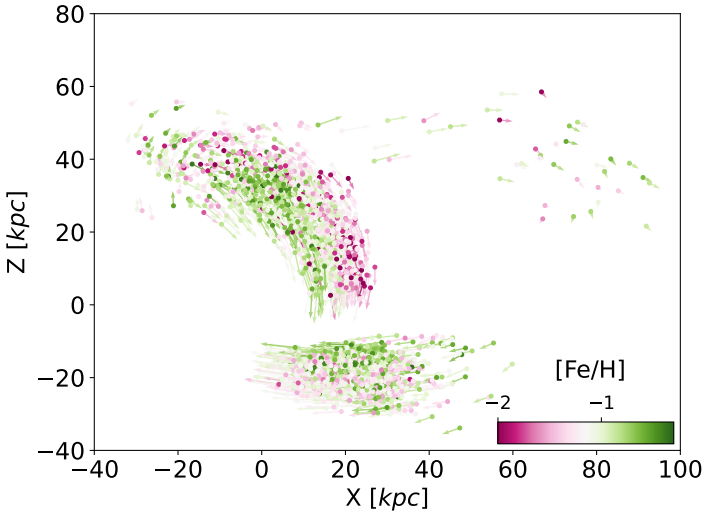

Fig. 5 Distribution of the mock data. The spatial distribution of the particles of simulation in the X-Z plane. Definitions of colors and arrows are consistent with those in Figure 1

to the research support. X.-X. X. and J. C. led the discussion. X.-X. X. and R.-Z. Z. selected the Sagttarius members from LAMOST DR8. B.-Q. Z. and Z.-H. Z. analyzed the data of MaNGA survey. Z.-X. G. and G.Z. have regular discussions. Z.-X. G., X.-X. X. and Z.-H. Z. co-wrote the initial manuscript. All authors discussed and commented on the manuscript.

Additional information

Correspondence and requests for materials should be addressed to Xiang-Xiang Xue, Chao Liu, or Gang Zhao.

Competing interest

The authors declare no competing interests.

Extended data

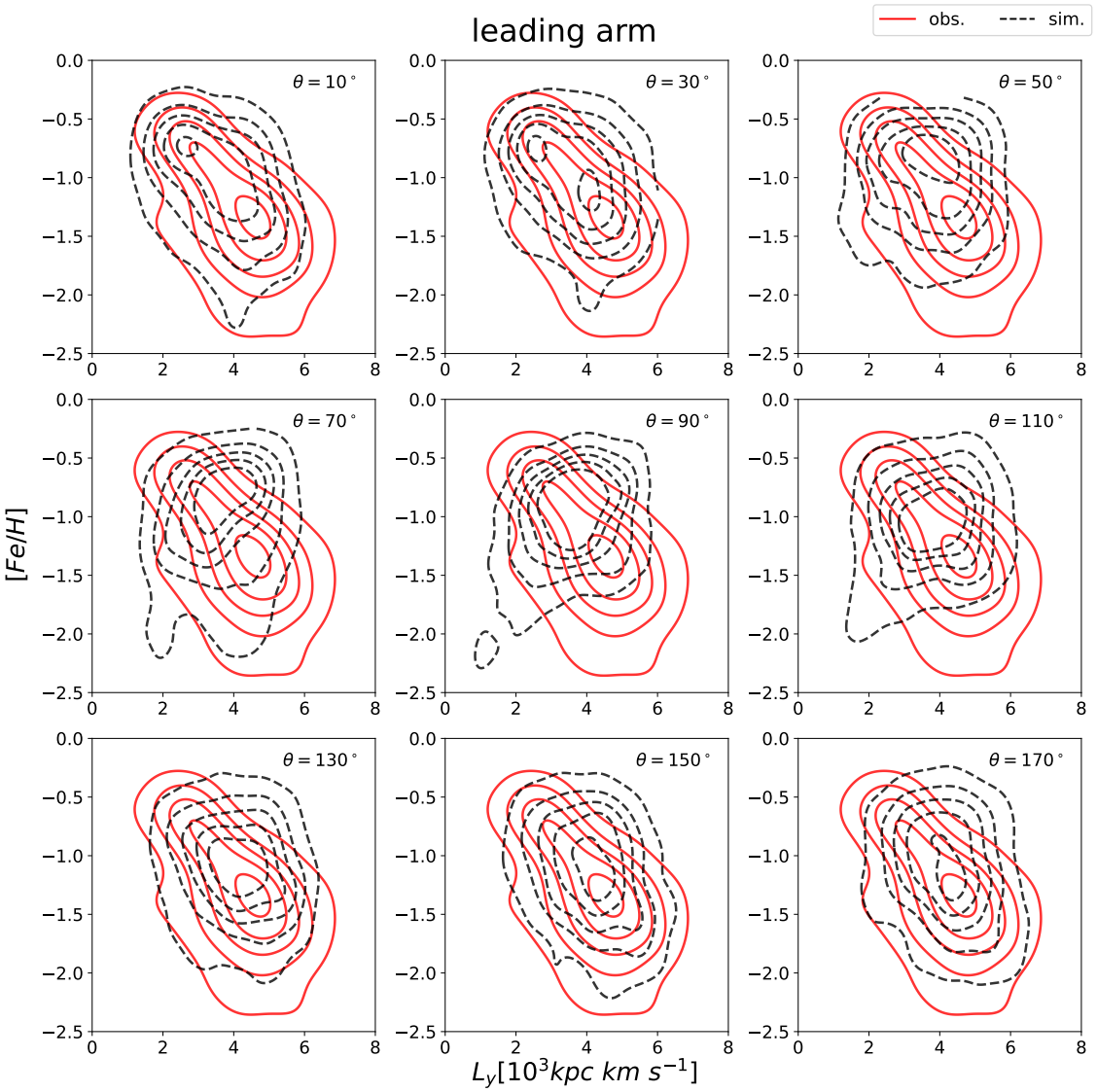

Fig. 6 The impact of different θ on leading arm. In these simulations, ϕ is taken as 0. The red contour represents the density of observation points, while the gray contour shows the distribution of points sampled from the simulation data.

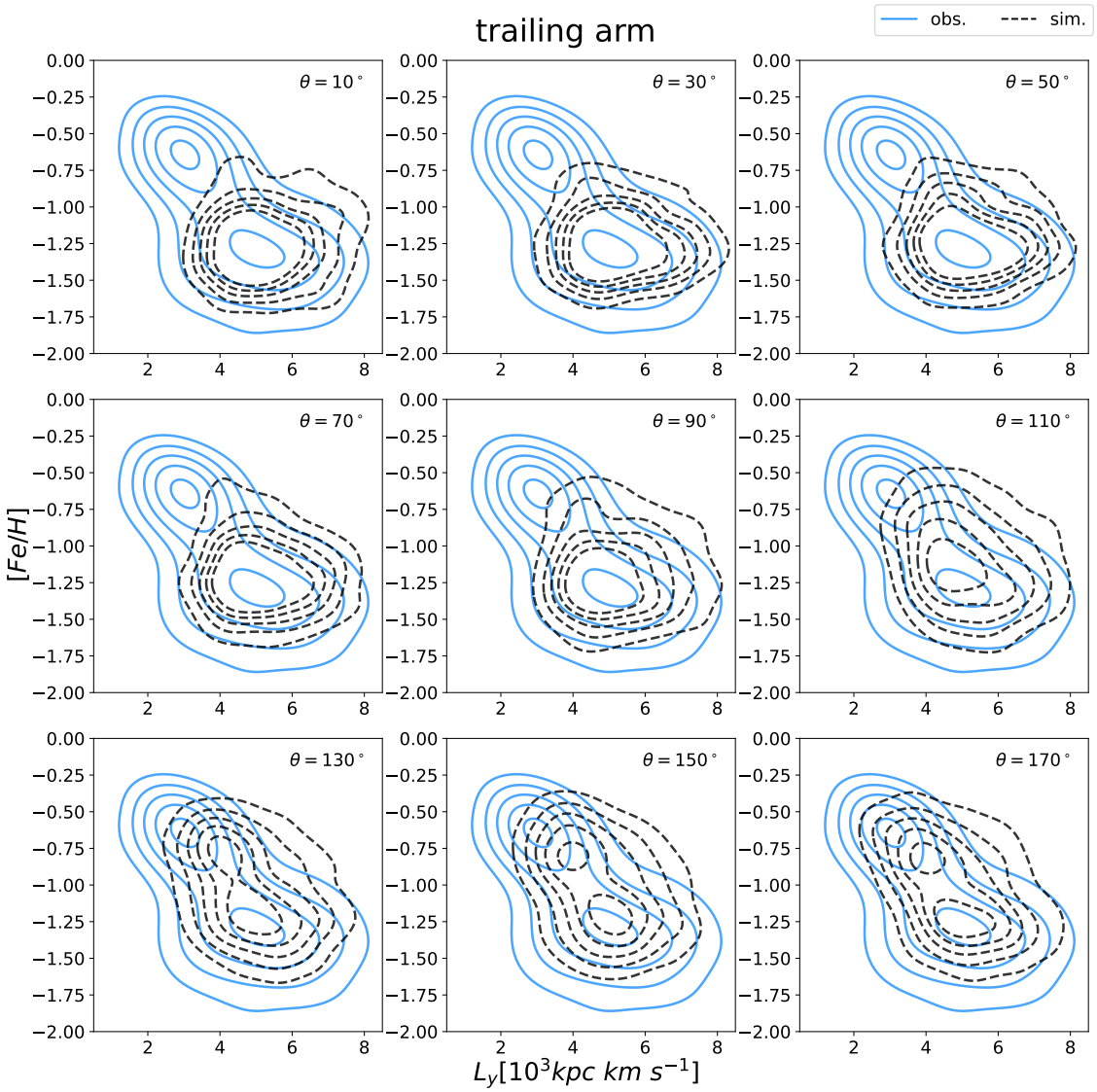

Fig. 7 The impact of different θ on trailing arm. In these simulations, ϕ is taken as 0. The blue contour represents the density of observation points, while the gray contour shows the distribution of points sampled from the simulation data.

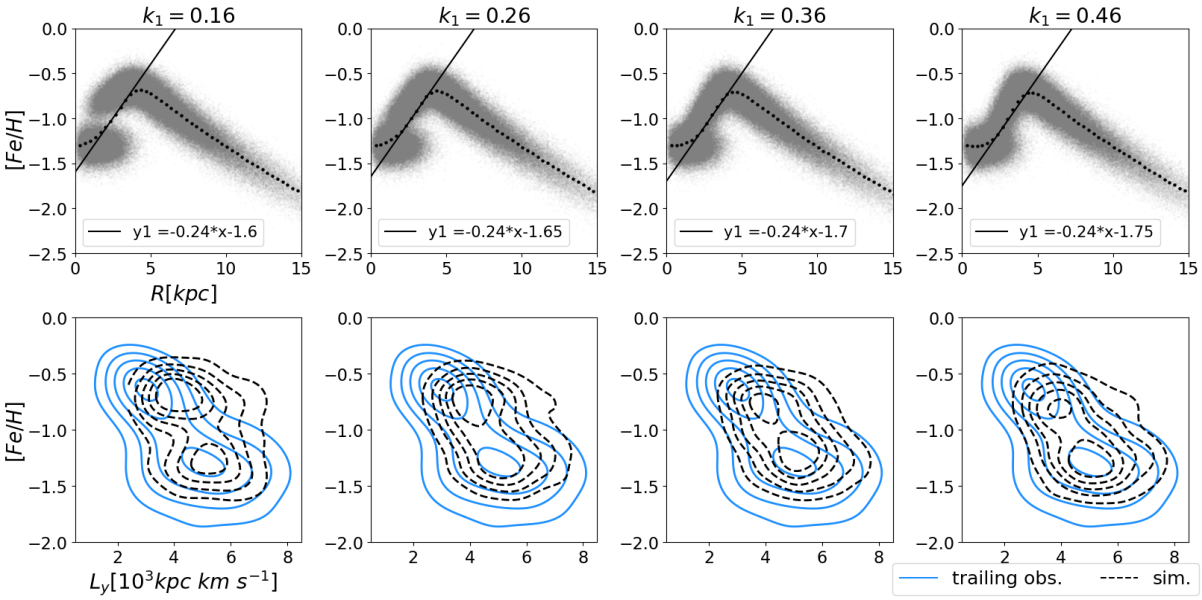

Fig. 8 The impact of k_1. The first row presents the variation of the initial metallicity of the Sgr disk with the radius R under different k1 values. In these models, the value of k_2 is set to 0.22. The second row shows the effect of different k1 values on the relationship between $[Fe/H]$ and L_y.

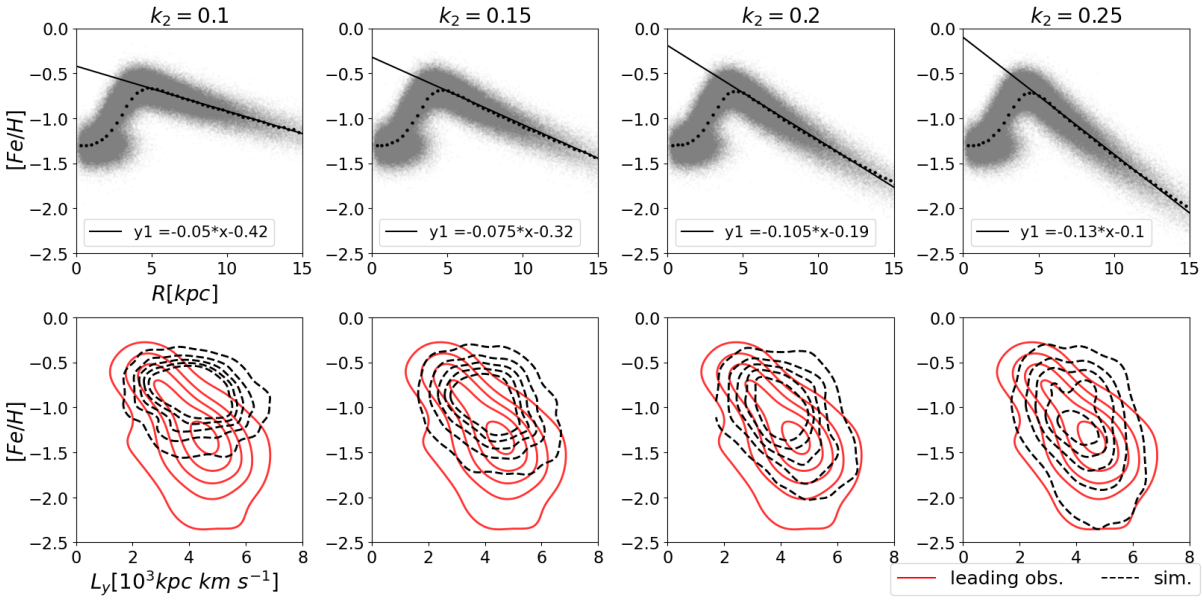

Fig. 9 The impact of k_2. The first row presents the variation of the initial metallicity of the Sgr disk with the radius R under different k2 values. In these models, the value of k_1 is set to 0.36. The second row shows the effect of different k2 values on the relationship between $[Fe/H]$ and L_y.

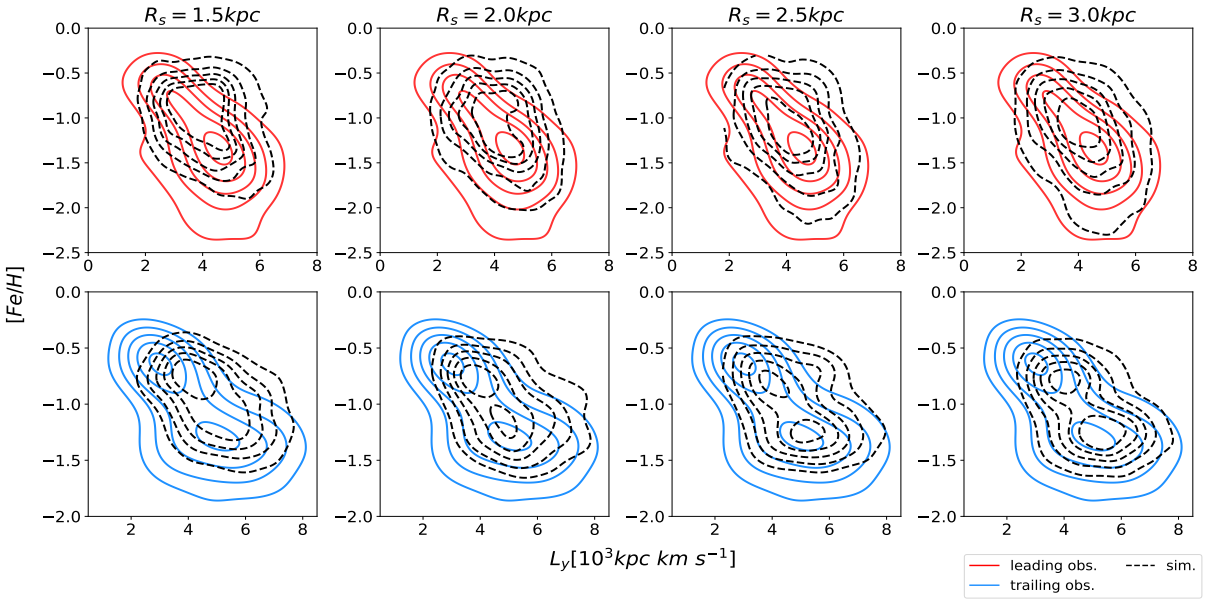

Fig. 10 The influence of scale length on stellar stream. R_S denotes the initial scale length of the Sgr model. The first row presents how the leading arm in the simulation varies with the scale length of the Sgr disk within the space of $[Fe/H]$ and L_y, and the second row shows how the mock data of the trailing arm varies with the scale length.

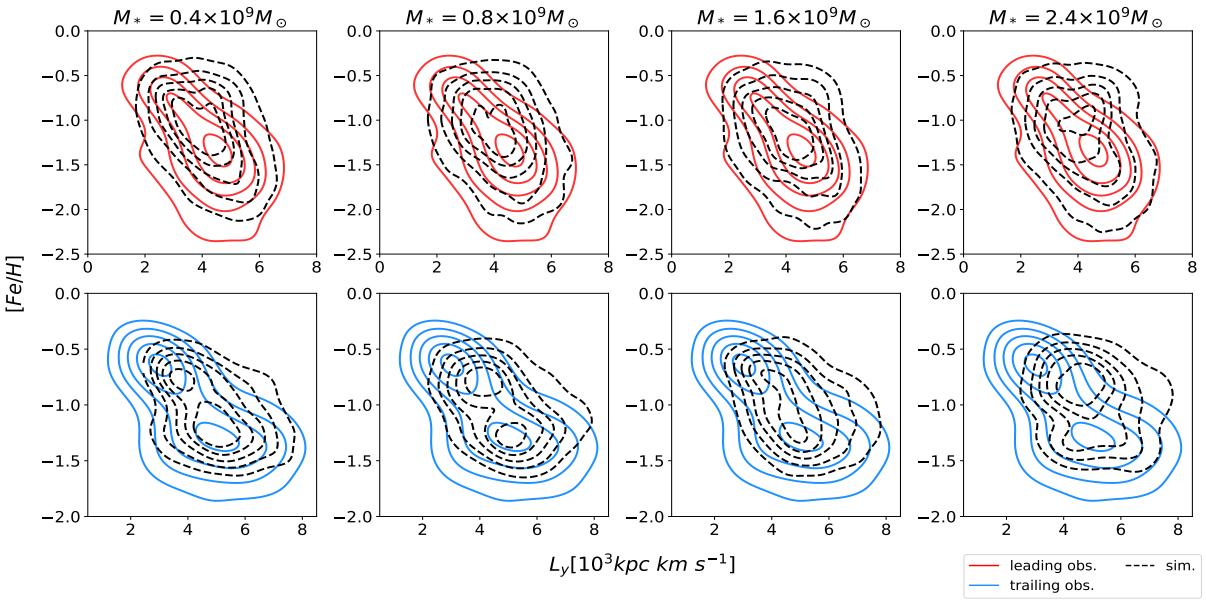

Fig. 11 The influence of mass on stellar stream. M_* denotes the stellar mass of the Sgr model. The first row presents how the leading arm in the simulation varies with the initial mass of the disk within the space of $[Fe/H]$ and L_y, and the second row shows how the mock data of the trailing arm varies with the initial mass.

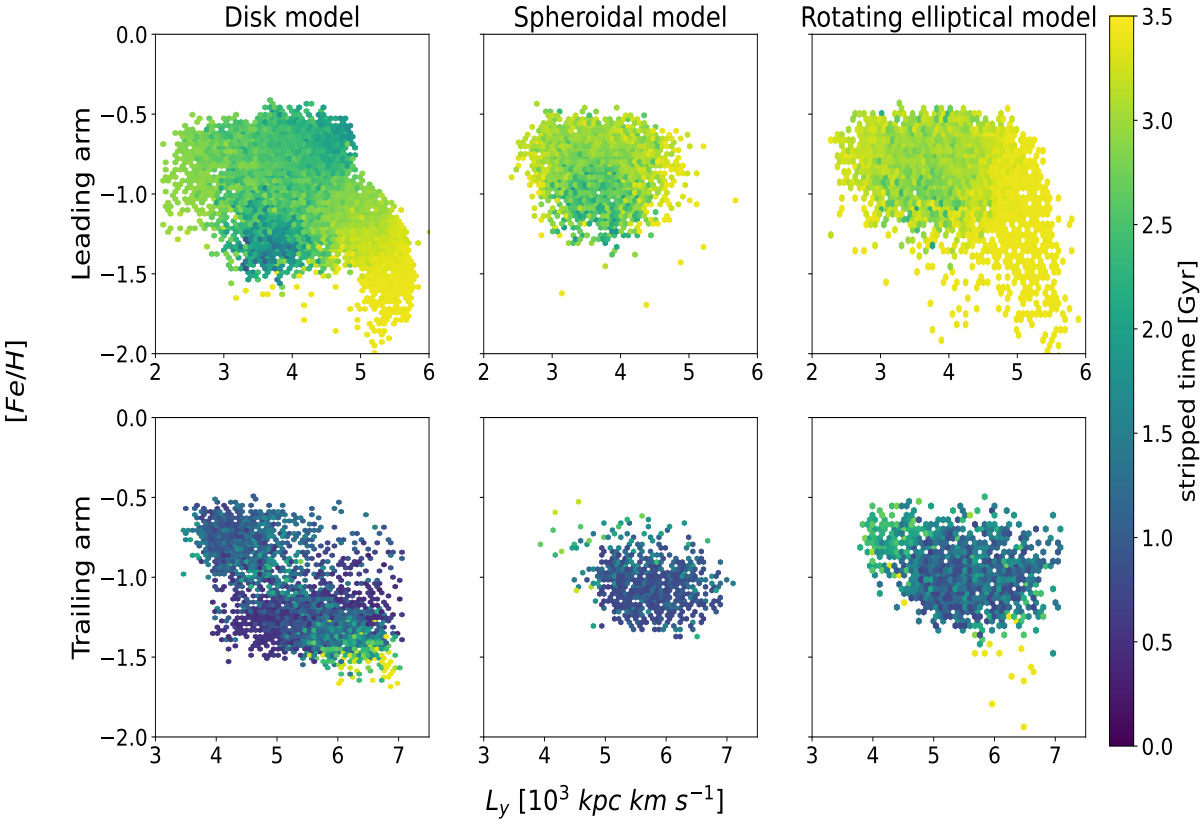

Fig. 12 Comparison of disk model, spheroidal model and rotating elliptical model. Top row: distribution of the leading arm generated by three models in the [Fe/H]-L_y space. The disk model adopts our fiducial model. **Bottom row:** the $[Fe/H] - L_y$ correlation of the traling arms. Each hexagonal bin represents the mean value of all data points within its corresponding region, and color represents the stripped time when the stellar particle left its progenitor. A larger stripped time indicates that the star is stripped earlier.

References

[1] Zhang, L. *et al.* A Catalog of Distance Determinations for the LAMOST DR8 K Giants in the Galactic Halo. *Astrono. J* **165**, 224 (2023).

[2] Navarro, J. F., Frenk, C. S. & White, S. D. M. A Universal Density Profile from Hierarchical Clustering. *Astrophys. J.* **490**, 493–508 (1997).

[3] Miyamoto, M. & Nagai, R. Three-dimensional models for the distribution of mass in galaxies. *Publ. Astron. Soc. Jpn.* **27**, 533–543 (1975).

[4] Bovy, J. galpy: A Python Library for Galactic Dynamics. *Astrophys. J. Suppl. Ser.* **216**, 29 (2015).

[5] Vasiliev, E. & Belokurov, V. The last breath of the Sagittarius dSph. *Mon. Not. R. Astron. Soc.* **497**, 4162–4182 (2020).

[6] Li, Z. *et al.* Exploring the ex-situ components within Gaia DR3. *Mon. Not. R. Astron. Soc.* **527**, 9767–9781 (2024).

[7] Wang, F. *et al.* Local stellar kinematics and Oort constants from the LAMOST A-type stars. *Mon. Not. R. Astron. Soc.* **504**, 199–207 (2021).

[8] Vasiliev, E., Belokurov, V. & Erkal, D. Tango for three: Sagittarius, LMC, and the Milky Way. *Mon. Not. R. Astron. Soc.* **501**, 2279–2304 (2021).

[9] Sheng, Y., Ting, Y.-S., Xue, X.-X., Chang, J. & Tian, H. Uncovering the first-infall history of the LMC through its dynamical impact in the Milky Way halo. *Mon. Not. R. Astron. Soc.* **534**, 2694–2714 (2024).

[10] Hernquist, L. An Analytical Model for Spherical Galaxies and Bulges. *Astrophys. J.* **356**, 359 (1990).

[11] Yurin, D. & Springel, V. An iterative method for the construction of N-body galaxy models in collisionless equilibrium. *Mon. Not. R. Astron. Soc.* **444**, 62–79 (2014).

[12] Springel, V. The cosmological simulation code GADGET-2. *Mon. Not. R. Astron. Soc.* **364**, 1105–1134 (2005).

[13] Penarrubia, J. *et al.* Was the Progenitor of the Sagittarius Stream a Disc Galaxy? *Mon. Not. R. Astron. Soc. Lett.* **408**, L26–L30 (2010).

[14] Oria, P.-A., Ibata, R., Ramos, P., Famaey, B. & Errani, R. Revisiting a Disky Origin for the Faint Branch of the Sagittarius Stellar Stream. *Astrophys. J. Lett.* **932**, L14 (2022).

[15] Toomre, A. & Toomre, J. Galactic Bridges and Tails. *Astrophys. J.* **178**, 623–666 (1972).

[16] Bundy, K. *et al.* Overview of the SDSS-IV MaNGA Survey: Mapping nearby Galaxies at Apache Point Observatory. *Astrophys. J.* **798**, 7 (2015).

[17] Sánchez, S. F. *et al.* Pipe3D, a pipeline to analyze Integral Field Spectroscopy Data: II. Analysis sequence and CALIFA dataproducts. *Rev. Mexicana Astron. Astrofis.* **52**, 171–220 (2016).

[18] Sánchez, S. F. *et al.* SDSS-IV MaNGA: pyPipe3D Analysis Release for 10,000 Galaxies. *Astrophys. J. Suppl. Ser.* **262**, 36 (2022).